

Updated fundamental constant constraints from Planck 2018 data and possible relations to the Hubble tension

Luke Hart^{1*} and Jens Chluba¹

¹Jodrell Bank Centre for Astrophysics, Alan Turing Building, University of Manchester, Manchester M13 9PL

Accepted –. Received –.

ABSTRACT

We present updated constraints on the variation of the fine structure constant, α_{EM} , and effective electron rest mass, m_e , during the cosmological recombination era. These two fundamental constants directly affect the ionization history at redshift $z \simeq 1100$ and thus modify the temperature and polarisation anisotropies of the cosmic microwave background (CMB) measured precisely with *Planck*. The constraints on α_{EM} tighten slightly due to improved *Planck* 2018 polarisation data but otherwise remain similar to previous CMB analysis. However, a comparison with the 2015 constraints reveals a mildly discordant behaviour for m_e , which from CMB data alone is found below its local value. Adding baryon acoustic oscillation data brings m_e back to the fiducial value, $m_e = (1.0078 \pm 0.0067) m_{e,0}$, and also drives the Hubble parameter to $H_0 = 69.1 \pm 1.2$ [in units of $\text{km s}^{-1} \text{Mpc}^{-1}$]. Further adding supernova data yields $m_e = (1.0190 \pm 0.0055) m_{e,0}$ with $H_0 = 71.24 \pm 0.96$. We perform several comparative analyses using the latest cosmological recombination calculations to further understand the various effects. Our results indicate that a single-parameter extension allowing for a slightly increased value of m_e ($\simeq 3.5\sigma$ above $m_{e,0}$) could play a role in the Hubble tension.

Key words: recombination – fundamental physics – cosmology – CMB anisotropies

1 INTRODUCTION

In the last few decades, we have achieved unprecedented cosmological results with the CMB anisotropies through various missions (Bennett et al. 2013; Planck Collaboration et al. 2014). The 2015 release of *Planck* gave us unparalleled precision on the temperature spectra and greatly improved polarisation data at small angular scales (Planck Collaboration et al. 2015a; et. al. 2016). With these modern day developments, we have opened a gateway to various extensions to the standard ΛCDM model. Several groups have studied cosmological limits on neutrino masses and the number of relativistic degrees of freedom, encoded in the N_{eff} parameter, leading to further discussion on the makeup of relativistic species in our universe (Gratton et al. 2008; Battye & Moss 2014). Similarly, the advances in CMB anisotropy data have allowed us to explore parameter space of Big Bang Nucleosynthesis as well as other physics beyond the standard model such as magnetic field heating (e.g., Shaw & Lewis 2010; Planck Collaboration et al. 2016), non-standard recombination (e.g., Rubiño-Martín et al. 2010; Farhang et al. 2013) and WIMP dark matter annihilation models (e.g., Galli et al. 2009a; Hütsi et al. 2009; Chluba 2010; Planck Collaboration et al. 2015a).

One of the many key physical processes that we can study during the recombination epoch is the possible variations of fundamental constants (Kaplinghat et al. 1999). Comprehensive re-

views that motivate the search for variations of fundamental constants have been given in the literature (Uzan 2003, 2011). For instance, constants such as the fine structure constant, α_{EM} , or the effective electron mass, m_e , can vary due to the introduction of non-standard electromagnetically-interacting fields (Bekenstein 1982). At low redshifts, these constants have been constrained with quasar absorption lines (Bonifacio et al. 2014; Kotuš et al. 2017; Murphy & Cooksey 2017) and more recently, direct measurements from the Large Magellanic Cloud (Levshakov et al. 2019). One study has tested variations of the fine structure constant using thermonuclear supernovae (Negrelli et al. 2018). In addition, several papers have studied the variations of these fundamental constants through their effect on the ionization history and the CMB anisotropies (Battye et al. 2001; Avelino et al. 2001; Scóccola et al. 2009; Menegoni et al. 2012; Planck Collaboration et al. 2015b).

In Hart & Chluba (henceforth HC17, 2018), we provided the *Planck* 2015 CMB constraints on constant variations of α_{EM} and m_e ¹, in detail modeling the effects using the cosmological recombination code *CosmoRec* (Chluba & Thomas 2011). There we also considered explicitly time-dependent variations of α_{EM} and m_e across the recombination epoch using a phenomenological power-

¹ The relative changes of m_e allows for a dimensionless rescaling of the rest mass of the electron during recombination, motivated by previous works (see Uzan 2011, for more details).

* Email: luke.hart@manchester.ac.uk

law in redshift (see HC17), that can be motivated with Mota & Barrow (2004). Spatial variations of the fine structure constant have also been discussed (Planck Collaboration et al. 2015b; Smith et al. 2019), as well as variations of the gravitational constant (Galli et al. 2009b; Alvey et al. 2019). So far, no significant departures from the expected values of fundamental constants have been reported.

For the 2018 release of CMB anisotropy results, the *Planck* team was able to significantly reduce remaining systematic effects in the large-scale data (Planck Collaboration et al. 2018c). Furthermore, polarised foregrounds were even more carefully subtracted in this recent analysis, leading to improved constraints from the CMB polarisation data (e.g., the reionisation optical depth Planck Collaboration et al. 2018a). The updated likelihood has not yet been used to constrain varying fundamental constants.

In this paper, we present the limits on the variations of fundamental constants as an update to the *Planck* 2015 constraints of HC17. Using the developments from the PR2 to the PR3 release of *Planck* data and benefiting from the reduction of systematics, especially in the *E*-mode polarisation, we derive the most stringent limits on the variations of fundamental constants from the CMB to date. These include limits on α_{EM} and m_e as well as their redshift-dependence. The general results for α_{EM} and m_e and their covariances are unaltered, however, we have expanded our discussion of the parameter degeneracies, and the interplay with the obtained Hubble parameter. This links to the apparent Hubble tension between low- and high-redshift probes (Riess et al. 2016; Bernal et al. 2016; Riess et al. 2019; Planck Collaboration et al. 2015a, 2018a), for which previous studies argued that variations of α_{EM} are unable to help much (Knox & Millea 2019). Similarly, variations of the atomic energy of hydrogen or its two-photon decay rate can only relieve the tension when both extensions are included, mainly at the cost of significantly increased uncertainties but without shifting the central value by much (Liu et al. 2019).

Here, we confirm that variations of α_{EM} indeed can only play minor role for the Hubble tension (see Fig. 1). However, a single-parameter extension that allows for variations of m_e indeed seems to alleviate the Hubble tension when combining various datasets at the cost of a discordant value for m_e during recombination and reionization². Indications for this behaviour were already seen for the *Planck* 2013 release (Planck Collaboration et al. 2015b), however, there the significance for the shift in m_e was at the $\approx 2\sigma$ level, while here we find a discrepant value of m_e at $\Delta m_e/m_e \approx 3.5\sigma$, thus calling for further investigation.

2 UPDATED CONSTRAINTS ON VARYING CONSTANTS

For this paper, the reference dataset is the 2018 baseline *Planck* data, with low- ℓ and high- ℓ data for temperature and *E*-mode polarisation power spectra, along with the lensing data from the same release (Planck Collaboration et al. 2019a, 2018b). This is also combined with baryon acoustic oscillation (BAO, Alam et al. 2015) and supernova/Cepheid variable (R19, Riess et al. 2019) data. In this section, we will focus the discussion on *Planck* and BAO data only and return to the effect of adding R19 data in Sect. 3.

As mentioned above, the large-angle polarisation data was slightly improved in the *Planck* 2018 data release; however, the reference *Planck* dataset too has changed. In previous *Planck* analyses the high- ℓ temperature and polarisation data was combined

with the low- ℓ temperature, *E* and *B*-mode polarisation data, along with the CMB lensing data as well. Here the *Planck* reference case includes just the high- ℓ and low- ℓ temperature and *E*-mode polarisation data with CMB lensing. We do not consider this posing an issue given the lack of constraining power from the *B*-modes for these fundamental constant variations.

Here, we examine α_{EM} and m_e , since these fundamental constants are the ones directly affecting the recombination process and Thomson scattering of the CMB. As illustrated in HC17, the main driving effect from a constant variation of α_{EM} is a change in the location of the last scattering surface. This originates from the main physical change to recombination from a varying fine structure constant, which modifies atomic transition energies, changing the temperature at which the photons and baryons decouple. Varying constants also affect specific transition rates such as Lyman- α and two-photon processes during recombination, though these modifications lead to far smaller changes (cf. HC17).

The effects from m_e on the recombination history are very similar, even if typically ≈ 2.5 times smaller than for a similar variation in α_{EM} . Marked differences in the way that the Thomson cross section is changed distinguishes α_{EM} from m_e variations. In particular, this effect strongly increases the geometric degeneracies between m_e and H_0 [throughout the paper in units of $\text{km s}^{-1} \text{Mpc}^{-1}$], leading to a significantly enhanced error on m_e from CMB data alone (HC17). The latter motivates a more careful consideration of the m_e constraints when combining CMB with external data, as we especially discuss in Sect. 3, where we present new results for both the *Planck* 2015 and 2018 releases.

2.1 Variations of the fine structure constant: α_{EM}

We find that the constraints on α_{EM} remain largely unchanged when moving to the *Planck* 2018 dataset, albeit yielding slightly improved errors. We summarized the changes through the various *Planck* data releases in Fig. 1. If we compare with the CMB-only values from our previous paper, we can see a change of the fine structure constant from $\alpha_{\text{EM}}/\alpha_{\text{EM},0} = 0.9993 \pm 0.0025$ to $\alpha_{\text{EM}}/\alpha_{\text{EM},0} = 1.0005 \pm 0.0024$. When we add BAO data, the value drifts slightly away from unity, $\alpha_{\text{EM}}/\alpha_{\text{EM},0} = 1.0019 \pm 0.0022$. This matches the behaviour found for the 2013 and 2015 data, as seen in Fig. 1, where the fiducial value of α_{EM} shifts to slightly higher values. The errors have not improved substantially due to the addition of higher-precision polarisation data, mainly affecting the reionization optical depth τ , which is largely uncorrelated with α_{EM} .

The values of the standard parameters when adding α_{EM} are presented in Table 1. The majority of the fiducial parameters' positions and errors stay the same except for n_s and $100\theta_{\text{MC}}$. The error in n_s increases by 0.7σ , however, the θ_{MC} error increases by an order of magnitude due to geometric degeneracies (e.g., Planck Collaboration et al. 2015b). The effect is not as dramatic in H_0 , where the error is only doubled due to the non-linear contributions from some of the other parameters diluting the increase in the error. This all follows the behaviour of the constraints when α_{EM} was added in previous works (Planck Collaboration et al. 2015b; Hart & Chluba 2018). Similarly, Table 1 shows that when adding BAO data, the limits do not change qualitatively, except the distance ladder contributions leading to $\sigma_{H_0} = 0.71$ while pulling H_0 slightly upwards.

A selection of the most-affected standard parameter posteriors is shown in Fig. 2, where we have compared the CMB-only 2015 (red) and 2018 posteriors (blue), along with respectively coloured bands, showing the fiducial 1σ limits of these parameters. The de-

² Though we focus on recombination here, the calculation of the reionization history is the standard calculation done within CAMB.

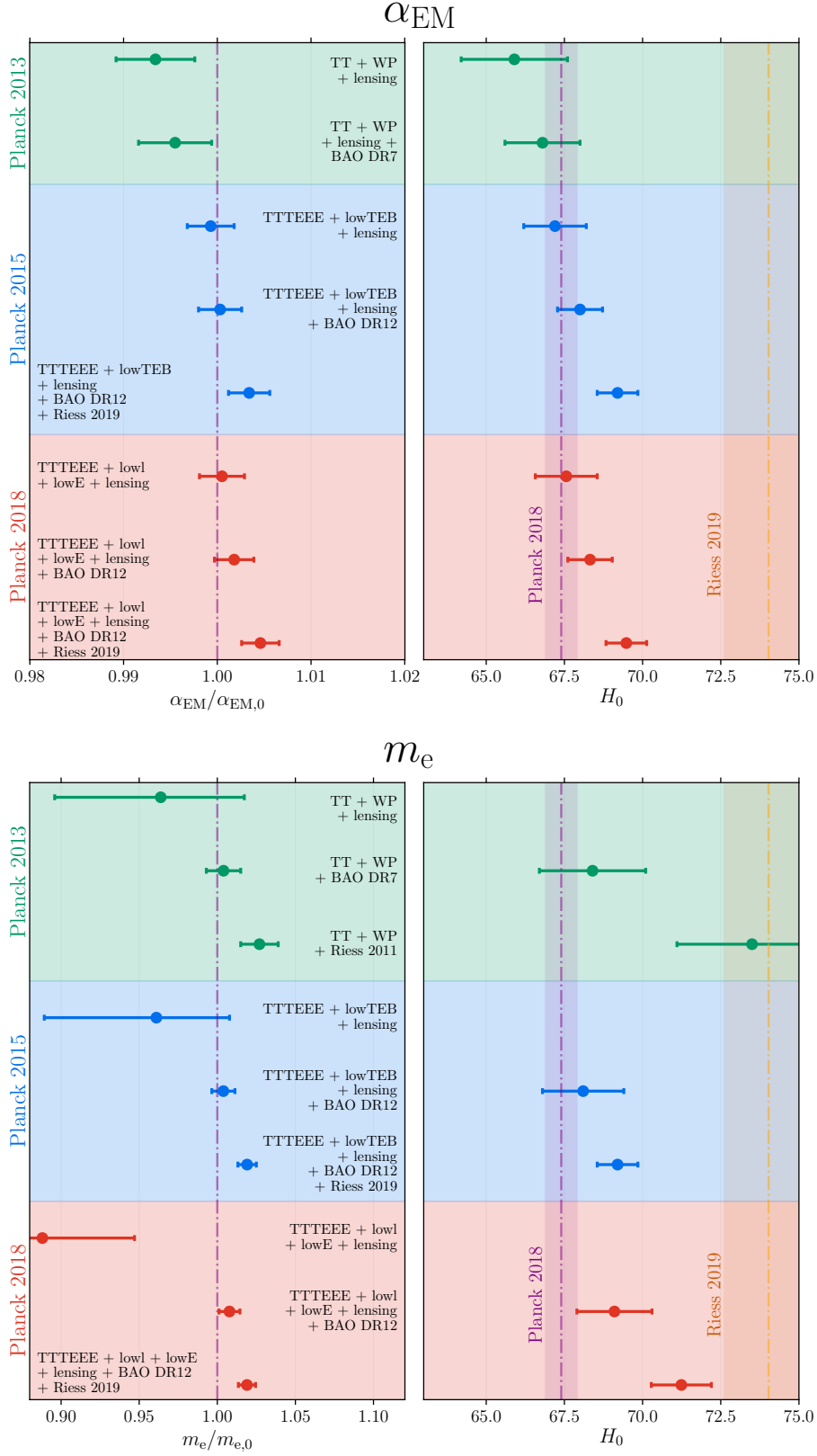


Figure 1. Constraints on the fundamental constants (*left*) using various combinations of *Planck* data included with their H_0 values and errors (*right*). The cases without R19 data are discussed in Sect. 2, while the addition of R19 data is considered in Sect. 3, when alluding to the Hubble tension. *Top*: results from the fine structure constant α_{EM} . *Bottom*: similar results but from the effective electron mass m_e . Here we have redacted the data from CMB data only because the error bars are so large for H_0 . For the m_e MCMC analysis, we have widened the prior on the Hubble constant such that $H_0 > 20$.

Parameter	<i>Planck</i> 2018	<i>Planck</i> 2018 + varying α_{EM}	<i>Planck</i> 2018 + BAO + varying α_{EM}	<i>Planck</i> 2018 + varying m_e	<i>Planck</i> 2018 + BAO + varying m_e
$\Omega_b h^2$	0.02237 ± 0.00015	0.02236 ± 0.00015	0.02240 ± 0.00014	$0.0199^{+0.0012}_{-0.0014}$	0.02255 ± 0.00016
$\Omega_c h^2$	0.1199 ± 0.0012	0.1201 ± 0.0014	0.1199 ± 0.0015	0.1058 ± 0.0076	0.1208 ± 0.0018
$100\theta_{\text{MC}}$	1.04088 ± 0.00031	1.0416 ± 0.0034	1.0436 ± 0.0030	0.958 ± 0.045	1.0464 ± 0.0047
τ	0.0542 ± 0.0074	0.0540 ± 0.0075	0.0553 ± 0.0075	0.0512 ± 0.0077	0.0549 ± 0.0074
$\ln(10^{10} A_s)$	3.044 ± 0.014	3.043 ± 0.015	3.043 ± 0.015	3.029 ± 0.017	3.045 ± 0.014
n_s	0.9649 ± 0.0041	0.9637 ± 0.0070	0.9621 ± 0.0070	0.9640 ± 0.0040	0.9654 ± 0.0040
$\alpha_{\text{EM}}/\alpha_{\text{EM},0}$	--	1.0005 ± 0.0024	1.0019 ± 0.0022	--	--
$m_e/m_{e,0}$	--	--	--	0.888 ± 0.059	1.0078 ± 0.0067
H_0	67.36 ± 0.54	67.56 ± 0.99	68.32 ± 0.71	46^{+9}_{-10}	69.1 ± 1.2

Table 1. Marginalised values of the fine structure constant and effective electron mass α_{EM} and m_e using the *Planck* 2018 data along with BAO contributions. We used a wide prior for H_0 so that the 1σ limit is not cut off and therefore avoids biasing the marginalised m_e posterior ($H_0 > 20$).

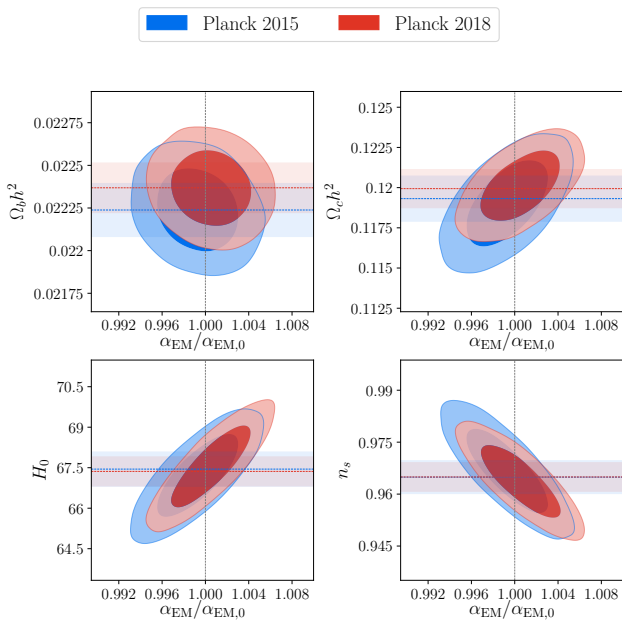


Figure 2. The posterior contours that illustrate the degeneracies between the fine structure constant α_{EM} and the most-affected standard parameters $\{\Omega_b h^2, \Omega_c h^2, H_0, n_s\}$. The ΛCDM scenario of $\alpha_{\text{EM}}/\alpha_{\text{EM},0} = 1.0$ is added as a reference, along with the 1σ values of *Planck* 2015 and 2018 standard parameters in coloured bands.

generacy with H_0 has not changed except that the locations of the contours have shifted to slightly larger marginalised values of H_0 , from $H_0 = 67.2 \pm 1.0$ in the 2015 release to $H_0 = 67.56 \pm 0.99$ in the 2018 release. This shift marks the main degeneracy of the α_{EM} parameter, however, we can also clearly see a degeneracy with the tilt of the spectrum, another parameter that slightly differs between the *Planck* releases. Comparing the fiducial bands in Fig. 2 with the locations of the contours, it is clear that the $\Omega_b h^2$ and $\Omega_c h^2$ contours have shifted in opposite directions to their 1σ bands between the two datasets. Overall, we find consistent results for all the parameters between the two *Planck* releases. Addition of BAO data to the analysis does not alter the conclusions significantly.

2.2 Variations of the effective electron mass: m_e

The difference in constraints for m_e is slightly more complicated than the picture for α_{EM} . Although there are improvements over the *Planck* 2015 results, the marginalised value of m_e is still heavily influenced by the prior definition of H_0 . This aspect was covered in our previous work, where we used a prior such that $H_0 > 40$ to conform with the initial CMB analysis with *Planck*, which combined *Planck* 2013 and *WMAP* data (Planck Collaboration et al. 2015b). However, when considering CMB-only 2018 constraints, the marginalised value of m_e slips further away from unity with H_0 departing from its fiducial CMB value. We thus used an even more extended prior $20 < H_0 < 100$ to avoid prior-domination.

For the CMB-only results presented in Table 1, we applied the aforementioned wide prior; however, we have instead shown the narrow prior results in Fig. 1 to better compare with previous works. Further discussion on the prior is found in Sec. 2.3, where we show the changes in the contours as the prior is adjusted. In 2013 and 2015, the CMB-only constraint for m_e were consistent with the standard value, given the large error bar due to geometric degeneracies. With the 2018 data, m_e drifts further below the local value, indicating a discrepancy of $\Delta m_e/m_e \simeq -2\sigma$ level, with extremely low value for H_0 (see Table 1). Although for the *Planck* 2013 and 2015 data, the value was consistent with $m_{e,0}$ to within 1σ , this behaviour is not surprising given the large degeneracies between H_0 and m_e already documented in previous works on *Planck* data and fundamental constant variations. Adding BAO data brings m_e back to the standard value, restoring concordance at a slightly improved error for the 2018 data.

While parameters like τ , n_s and A_s all stay within 1σ of ΛCDM when adding m_e , we must appreciate the drifts in the baryonic and cold matter density parameters, $\Omega_b h^2$ and $\Omega_c h^2$. From Fig. 3 and Table 1, we can see the sharp degeneracies of these parameters leading to $\simeq -1.8\sigma$ drifts in $\Omega_c h^2$ and $\simeq -2\sigma$ for $\Omega_b h^2$ for CMB-only constraints. These shifts are due to correlations with H_0 (through the well-known $H_0 - \Omega_m$ degeneracy). When adding BAO data, concordance with ΛCDM is again restored to within $\simeq 1\sigma$ (see Table 1).

2.2.1 Electron mass dependence of the Thomson cross section

As highlighted in HC17, the effect of m_e on the Thomson scattering cross section, $\sigma_{\text{T}} \propto \alpha_{\text{EM}}^2/m_e^2$, plays a distinct role for the geometric degeneracies of α_{EM} and m_e . The primary effect from the rescaling of σ_{T} , outside of the recombination fraction, arises from the rescaling of the Thomson visibility function $g(z)$. This was discussed in HC17. For α_{EM} , the rescaling of σ_{T} improves the obtained error at

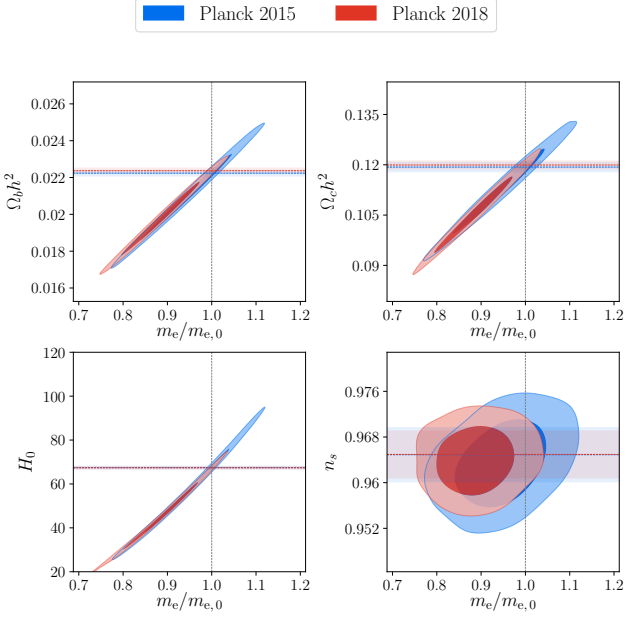


Figure 3. Same as Fig. 2 except here we show the contours for m_e . The same Λ CDM reference marker and fiducial cosmology 1σ bands have been added here. In these contours we ensured $20 < H_0 < 100$.

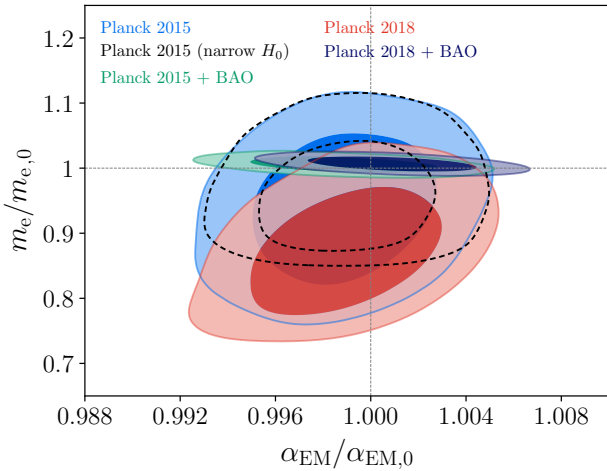


Figure 4. Posterior contours between α_{EM} and m_e for the *Planck* 2015 and 2018 data along with BAO contributions. Note that the dashed contour shows the 2015 contour but with a tighter prior on $H_0 \in [40, 100]$.

the level of $\approx 30\%$, while for m_e it opens up the geometric degeneracy: if we do not include the effects on σ_T , the constraint changes from $m_e/m_{e,0} = 0.888 \pm 0.059$ to $m_e/m_{e,0} = 1.0005 \pm 0.0099$. In this case, we also regain a value of $H_0 = 67.5 \pm 1.7$, with an increased overall error but very close to the *Planck* value of $H_0 = 67.36 \pm 0.54$. The main impacts from omitting σ_T come from low redshift changes in the visibility function, which give the m_e parameter a stronger correlation with H_0 . Overall, this highlights that variations of m_e , through the distinct effect on the Thomson optical depth open the geometric degeneracy line, an aspect that we will return to in Sect. 3.

2.3 Joint variations of α_{EM} and m_e

In Fig. 4, we present the contours when α_{EM} and m_e are both allowed to vary. Here we present the posteriors for CMB-only and *Planck* 2018 + BAO, also comparing with the *Planck* 2015 results. Without BAO data, m_e assumes values $< m_{e,0}$, covering a wide range reaching down to $m_e/m_{e,0} \approx 0.75$ at 2σ , as also found without extra variation of α_{EM} (see Table 1). The two-dimensional posterior is highly non-Gaussian in this case and for the 2018 data we can even notice some truncation due to the assumed H_0 prior at the lower end of the contour. This is illustrated for the 2015 data run (dashed contours in Fig. 4), mimicking the initial *Planck* analysis (Planck Collaboration et al. 2015b). Similar to the *Planck* paper, we see no strong degeneracy between α_{EM} and m_e and this is due to the improvements in the damping tail data which is explained in that paper.

The introduction of BAO data tightens the constraints on m_e and we can also observe a small drift in α_{EM} . The obtained value changes from $\alpha_{EM}/\alpha_{EM,0} = 0.9989 \pm 0.0026$ for the 2015 data to $\alpha_{EM}/\alpha_{EM,0} = 1.0010 \pm 0.0024$ with 2018 data, both with BAO included and when simultaneously varying m_e . By contrast, there is no drift for m_e , with $m_e/m_{e,0} = 1.0056 \pm 0.0080$ changing to $m_e/m_{e,0} = 1.0054 \pm 0.0080$ for *Planck* 2015+BAO and *Planck* 2018+BAO, respectively.

2.4 Constraints on α_{EM} and m_e with time dependence

Low redshift probes of fundamental constants have shown that possible variations would have to be as small as $\sim 10^{-6}$ today (see the review in Uzan 2011, for more details). However explicitly redshift-dependent variations have been motivated by a number of theoretical models such as the string dilaton and runaway dilaton models (Martins et al. 2015). Here we consider how the fundamental constants C vary with redshift across the recombination epoch, using the phenomenological parametrisation

$$C(z) = C_0 \left(\frac{1+z}{1100} \right)^p, \quad (1)$$

where $C \in \{\alpha_{EM}, m_e\}$ for this analysis. Time-independent variations are captured by constant change to C_0 , just as in the previous sections. Varying p parametrises the time-dependence. Here our reference value reflects the Λ CDM value to study the unique variations by pivoting around the maxima of the Thomson visibility function. It leaves the position of the Thomson visibility function practically unaltered while broadening and narrowing it for negative and positive values of p , respectively (Full details of the power law effects during recombination are found in Hart & Chluba (2018)).

When we add time-dependent variations using the power-law model in Eq. (1) to the MCMC analyses discussed in Sections 2.1 and 2.2, we obtain the results summarized in Table 2. In comparison to *Planck* 2015, the obtained central values and errors change marginally when p is added, showing no indication for departures from $p \approx 0$. Whilst $\alpha_{EM} = 0.9998 \pm 0.0036$ and $p = 0.0007 \pm 0.0036$ for the *Planck* 2015 release, the fundamental constant marginalised values are $\alpha_{EM} = 0.9997 \pm 0.0035$ and $p = -0.0011 \pm 0.0035$ for the *Planck* 2018 data. The index of the power law p , is consistent with zero to within $\sim 0.3\sigma$, suggesting that this parameter is tightly constrained by the current CMB anisotropies. Adding BAO data, we obtain $p = 0.0007 \pm 0.0031$, agreeing with the value for Λ CDM to within $\approx 0.2\sigma$. The overall posteriors remain extremely close to those presented in the *Planck* 2015 analysis, so that we do not repeat them here.

Parameter	<i>Planck</i> 2018 + varying $\alpha_{EM}(z, p)$	<i>Planck</i> 2018 + BAO + varying $\alpha_{EM}(z, p)$	<i>Planck</i> 2018 + varying $m_e(z, p)$	<i>Planck</i> 2018 + BAO + varying $m_e(z, p)$
$\Omega_b h^2$	0.02233 ± 0.00018	0.02243 ± 0.00016	$0.0197^{+0.0012}_{-0.0015}$	0.02254 ± 0.00019
$\Omega_c h^2$	0.1198 ± 0.0017	0.1201 ± 0.0017	$0.1045^{+0.0074}_{-0.0082}$	0.1209 ± 0.0019
$100\theta_{MC}$	1.0405 ± 0.0049	1.0441 ± 0.0038	0.950 ± 0.046	1.0466 ± 0.0049
τ	0.0545 ± 0.0077	0.0549 ± 0.0076	0.0513 ± 0.0081	0.0544 ± 0.0075
$\ln(10^{10} A_s)$	3.044 ± 0.015	3.043 ± 0.015	3.030 ± 0.018	3.044 ± 0.016
n_s	0.9640 ± 0.0071	0.9622 ± 0.0069	0.9655 ± 0.0064	0.9645 ± 0.0066
$\alpha_{EM}/\alpha_{EM,0}$	0.9997 ± 0.0035	1.0022 ± 0.0027	--	--
$m_e/m_{e,0}$	--	--	$0.878^{+0.057}_{-0.065}$	1.0081 ± 0.0070
p	-0.0011 ± 0.0035	0.0007 ± 0.0031	0.0014 ± 0.0043	-0.0007 ± 0.0043
H_0	67.3 ± 1.4	68.45 ± 0.88	44^{+9}_{-10}	69.1 ± 1.2

Table 2. Marginalised parameter values for MCMC runs with *Planck* data along with the power law defined in Equation (1). Both α_{EM} and m_e are shown with the constrained power law parameter along with the limit when BAO is added as well.

Turning to the case of time-varying m_e , we again find that p is consistent with zero at a fraction of a σ (see Table 2). Even with the large geometric degeneracies between H_0 and m_e described in Sec. 2.2, the only differences are small shifts of the central parameter values, which derive from the subtle differences in the effects between α_{EM} and m_e on the recombination and reionization visibilities mentioned above (see Sect. 2.2.1).

Our findings again highlight that explicitly time-varying α_{EM} and m_e can be constrained independently of their constant variations using CMB data. A more in depth study is thus expected to lead constraints on at least two independent model parameters if the recombination physics of the $z \approx 1100$ Universe is indeed affected.

3 ADDING SHOES DATA AND THE HUBBLE TENSION

Although the degeneracy between distance measures such as H_0 and α_{EM} is already evident, the geometric effects due to the scaling of the Thomson cross section creates an even larger degeneracy between m_e and H_0 , as well as the baryonic and cold dark matter densities ($\Omega_b h^2$ and $\Omega_c h^2$). We should thus check if the widening error bars of H_0 and m_e , as explained in Sec. 2.2, allow us to alleviate some of the recently discussed tensions with supernovae data (e.g. Riess et al. 2016; Bernal et al. 2016; Knox & Millea 2019).

In this section, we add SH0ES data (hereafter referred to as R19) to the analysis using a prior of $H_0 = 74.03 \pm 1.42$ (Riess et al. 2019). Our results are summarized in Fig. 1 and Table 3. We explicitly do not include fundamental constant variations in the low redshift data as we are simply studying the capability for these variations during recombination. When varying α_{EM} , a slight shift towards $\alpha_{EM}/\alpha_{EM,0} > 1$ is seen both for the *Planck* 2015+BAO+R19 and *Planck* 2018+BAO+R19 data. In addition, the derived value for H_0 moves towards the value preferred by the R19 data. However, the overall shifts remain $\lesssim 3\sigma$ when allowing α_{EM} to vary. This indicates that α_{EM} variations alone cannot fully reconcile the low- and high-redshift probes of the cosmological expansion rate.

In contrast, when we look at the results for m_e with added R19 measurements, the Hubble constant shifts to $H_0 = 71.24 \pm 0.96$, bringing it to within $\approx 2\sigma$ of the R19 value for the *Planck* 2018+BAO+R19 combination. For this case, the effective electron mass is $m_e/m_{e,0} = 1.0190 \pm 0.0055$, which indicates a $\approx 3.5\sigma$ tension with the Λ CDM value. This begs the question whether m_e could indeed play a role in the Hubble tension.

To understand this result a little better, we show the $m_e - \alpha_{EM}$

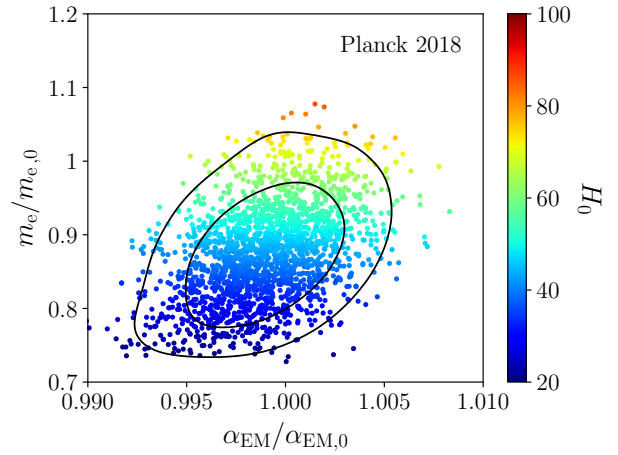


Figure 5. Two dimensional posteriors for α_{EM} and m_e with the values of H_0 for the given samples shown in colour for *Planck* 2015 (upper panel) and *Planck* 2018 (lower panel). The prior was set to $20 < H_0 < 100$, slightly affecting the lower end of posterior.

contour for the *Planck* 2018+BAO dataset, highlighting the corresponding value of H_0 in colour. As expected, the value of α_{EM} does not exhibit any strong preference on the value of H_0 , while m_e is strongly correlated. As mentioned in Sect. 2.2.1, the distinct role of σ_T opens the geometric degeneracy line when m_e is allowed to vary, which without rescaling σ_T is not present (HC17). When adding R19 data, the direction towards higher values of H_0 opens, allowing m_e to settle at $m_e/m_{e,0} > 1$ with R19 data is added.

To further assess the situation, we also looked at the total χ^2 from the marginalised result and compared the two cases of adding α_{EM} and m_e to the reference cases of CMB + BAO and CMB + BAO + R19. The low positive variation of α_{EM} coupled with the negative $\Delta\chi^2$ values shown in Table 3 indicate that the goodness-of-fit is not severely sacrificed when we add α_{EM} and m_e . For the CMB + BAO case, adding α_{EM} gives a slightly worse fit but m_e gives a marginally better fit. When we add R19 data, the χ^2 drops for both α_{EM} and m_e . We also find that the CMB-only component of the total χ^2 decreases when adding m_e to CMB+BAO+R19 such that $\Delta\chi^2_{CMB} = -1.17$. This means the goodness-of-fit improves for the CMB+BAO+R19 when m_e variations included. A detailed comparison of the χ^2 values is given in Table 4.

Parameter	<i>Planck</i> 2018 + BAO	<i>Planck</i> 2018 + BAO + α_{EM}	<i>Planck</i> 2018 + BAO + m_e	<i>Planck</i> 2018 + BAO + R19	<i>Planck</i> 2018 + BAO + R19 + α_{EM}	<i>Planck</i> 2018 + BAO + R19 + m_e
$\Omega_b h^2$	0.02244 ± 0.00013	0.02240 ± 0.00014	0.02255 ± 0.00016	0.02255 ± 0.00013	0.02244 ± 0.00014	0.02277 ± 0.00015
$\Omega_c h^2$	0.11895 ± 0.00092	0.1199 ± 0.0015	0.1208 ± 0.0018	0.11791 ± 0.00090	0.1204 ± 0.0014	0.1229 ± 0.0017
$100\theta_{MC}$	1.04100 ± 0.00029	1.0436 ± 0.0030	1.0464 ± 0.0047	1.04116 ± 0.00029	1.0475 ± 0.0027	1.0543 ± 0.0038
τ	0.0571 ^{+0.0067} _{-0.0076}	0.0553 ± 0.0075	0.0549 ± 0.0074	0.0602 ^{+0.0069} _{-0.0078}	0.0551 ± 0.0074	0.0533 ± 0.0074
$\ln(10^{10} A_s)$	3.048 ± 0.015	3.043 ± 0.015	3.045 ± 0.014	3.052 ^{+0.014} _{-0.015}	3.039 ± 0.015	3.044 ± 0.014
n_s	0.9674 ± 0.0037	0.9621 ± 0.0070	0.9654 ± 0.0040	0.9700 ± 0.0036	0.9567 ± 0.0066	0.9640 ± 0.0041
$\alpha_{EM}/\alpha_{EM,0}$	--	1.0019 ± 0.0022	--	--	1.0047 ± 0.0020	--
$m_e/m_{e,0}$	--	--	1.0078 ± 0.0067	--	--	1.0190 ± 0.0055
H_0	67.81 ± 0.42	68.32 ± 0.71	69.1 ± 1.2	68.32 ± 0.41	69.48 ± 0.65	71.24 ± 0.96
$\Delta\chi^2_{min}$	--	0.21	-0.39	--	-4.71	-10.92

Table 3. *Planck* 2018 marginalised results for varying α_{EM} and m_e along with BAO and R19 datasets. Reference cases for CMB+BAO and CMB+BAO+R19 are included. We also show the change in fit, $\Delta\chi^2_{min}$, for the results compared to their reference cases.

The tendency to allow for larger values of m_e and H_0 is even clear in the *Planck* 2013 data release (Planck Collaboration et al. 2015b) when combined with the 2011 SN data (Riess et al. 2011). Though the migration of both m_e and H_0 is larger for *Planck* 2013 (see Fig. 1), the value of m_e is only 2.3σ away from Λ CDM and no significant Hubble tension was yet identified back then. We find a similar constraint on m_e as for *Planck* 2018 when we consider a combination of *Planck* 2015+BAO+R19 data, $m_e/m_{e,0} = 1.0191 \pm 0.0059$ ($\Delta m_e/m_e \approx 3.2\sigma$); however, the movement of H_0 remains more restricted, leaving a $\approx 3.4\sigma$ tension with the R19 data (cf. Fig. 1). This indicates that for the *Planck* 2018 data the geometric degeneracy line is opened more strongly when allowing m_e to vary.

In Fig. 6, we show the contours of some of the most affected standard parameters. A full set of parameter contours is shown in Appendix A. The contours shift away from the CMB-only posteriors (blue bands) as BAO (red) and R19 (green) data are added. The $H_0 - m_e$ contour is narrower as R19 data is added and as described above, weighted more towards the R19 only value. We can see similar effects in $\Omega_b h^2$ and $\Omega_c h^2$, which move by $\approx 2.5\sigma$ and $\approx 1.8\sigma$, respectively. All this indicates that a discordant value of m_e can be traded in for an alleviation of the H_0 tension while affecting the standard parameters at the level of $\lesssim 2.3\sigma$.

Finally, the analysis with both m_e and α_{EM} varying can be extended to include R19 data as shown in Fig. 7. Here we have redone the analysis from Fig. 4, however the *Planck*-only contours have been removed for clarity. Though there is a small drift in α_{EM} , the main effect from adding R19 constraints is a migration of m_e away from the standard value. This is also expected from Fig. 5 and further supports the perspective that variations of m_e could indeed play a direct role in explaining the Hubble tension.

4 CONCLUSION

We provided updated constraints on the variation of the fundamental constants α_{EM} and m_e , closely following the discussion of HC17 for *Planck* 2015 data. When omitting Riess 2019 data, we find no significant difference between the results of the 2015 and the present analysis for variations of α_{EM} and m_e (see Fig. 1). As expected, the addition of improved polarisation information from *Planck* 2018 leads to slightly improved errors on α_{EM} and m_e with shifts between the values from the 2015 and 2018 data combina-

<i>Planck</i> 2018 + BAO	Λ CDM	+ $\Delta\alpha_{EM}$	+ Δm_e
<i>Planck</i> (high- ℓ +low- ℓ)	2789.36	2790.04	2789.50
BAO	8.61	8.14	8.08
$\Delta\chi^2$	--	0.21	-0.39
<i>Planck</i> 2018 + BAO + R19	Λ CDM	+ $\Delta\alpha_{EM}$	+ Δm_e
<i>Planck</i> (high- ℓ +low- ℓ)	2791.65	2792.65	2790.48
BAO	7.59	7.65	9.77
R19	16.25	10.48	4.31
$\Delta\chi^2$	--	-4.71	-10.92

Table 4. Changes in the goodness-of-fit χ^2 when α_{EM} or m_e is added to the Λ CDM model. Here the Λ CDM cases are references to compare the $\Delta\chi^2$ from each of the added fundamental constant variations. All the quoted χ^2 values are the fits from the final marginalised results quoted in Table 3.

tions remaining below $\approx 1\sigma$ (see Table 1 and 2 for summary of the parameter values).

In addition to the update of the *Planck* 2015 analyses, we also extended the discussion to combinations including R19 data (Sect. 3). R19 data pulls both α_{EM} and m_e above their standard values; however, only for the combination *Planck* 2018+BAO+R19 does the migration exceed the 3σ threshold (see Fig. 1 and Table 3). Simultaneously, we find the value for H_0 to move closer to that obtained from R19 data. Improvements in the χ^2 -values further indicate that variations of m_e could indeed play a role in the low- versus high-redshift Hubble tension.

As already alluded to in HC17, the distinct role of m_e in the value of $\sigma_T \approx \alpha_{EM}^2/m_e^2$ opens the geometric degeneracy line to enable R19 data to overcome the tight grip of *Planck* data on H_0 . When neglecting the rescaling of σ_T with m_e this degree of freedom closes. Our analysis thus suggests that a delicate interplay between the low- and high-redshift ionization history could indeed influence our interpretation of the cosmological datasets. A shift of m_e away from the standard value appears to enable this. More general alternatives could be a modified recombination history and simultaneously altered reionization history. Future works should thus investigate a possible integration of the reionization and recombination processes to more accurately model fundamental constant variations across cosmic time.

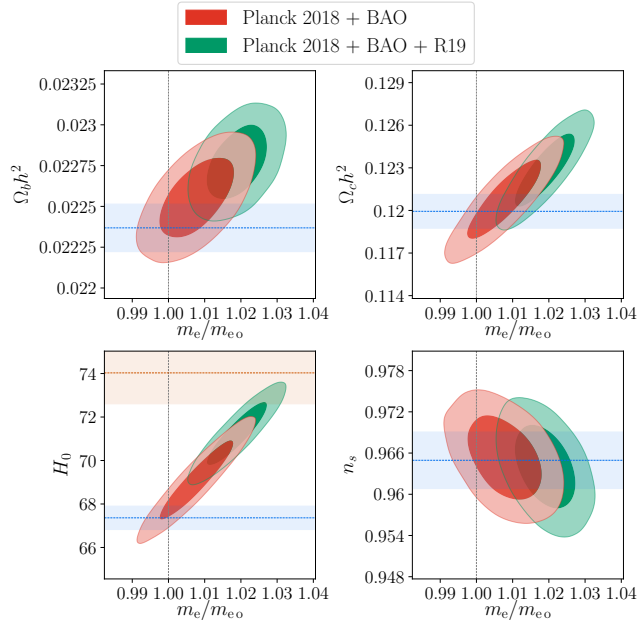


Figure 6. Marginalised contours from m_e with the standard parameters $\{\Omega_b h^2, \Omega_c h^2, H_0\}$. The other parameters have been omitted as they do not vary with the m_e changes and we have shown this in Fig. A1. The blue bands represent the standard Λ CDM limits for these parameters. The orange band represents the R19 constraint on H_0 (Riess et al. 2019).

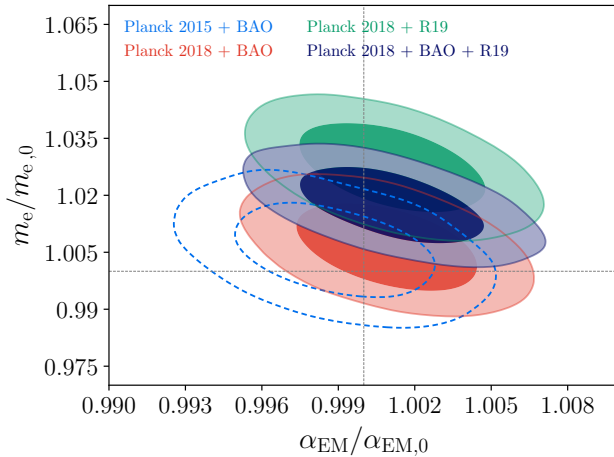


Figure 7. Probability contours between α_{EM} and m_e for *Planck* and BAO, with added R19 constraints as well.

Models with explicit time-dependence of α_{EM} and m_e should furthermore be more carefully studied. As pointed out in Poulin et al. (2019), models of early-dark energy could also play a role in the Hubble tension. Similar physical mechanisms could give rise to varying constants, potentially linking the effects to the same underlying scalar field. Recently, models with positive spatial curvature have too enriched the discussion on the Hubble tension (Di Valentino et al. 2019). Including fundamental constant variations may alleviate the discrepancies in lensing in a similar way to that of a closed Universe. Also, spatial variations of fundamental constants could be present, potentially linking the CMB anomalies seen at large-angular scales (Planck Collaboration et al. 2019b;

Smith et al. 2019). We look forward to exploring these possibilities in the future.

Finally, we stress that there seems to be a marked difference between the *Planck* 2015 and 2018 data. For *Planck* 2015, we find similar constraints on m_e but the shift in the Hubble parameter is more mild and unable to reconcile H_0 (see Fig. 1). This indicates that improvements to the *Planck* 2018 polarization data opened the aforementioned geometric degeneracy more strongly. This calls for further investigations of systematic effects to clearly identify the origin of our findings regarding the Hubble tension.

ACKNOWLEDGMENTS

We would like to thank Richard Battye and Aditya Rotti for helpful discussions. We would also like to thank Antony Lewis for his continued support whilst using the *CosmoMC* MCMC code and Eleonora Di Valentino for advice on the use of the *Planck* 2018 likelihood code. We would like to thank Silvia Galli for useful discussions surrounding fundamental constants and the *Planck* likelihood. We thank Vivian Poulin for interesting discussions surrounding the Hubble tension and useful extensions to the analysis. We would like to thank the reviewer for their helpful feedback regarding fundamental constant models and transparency. LH was funded by the Royal Society through grant RG140523. JC was supported by the Royal Society as a Royal Society University Research Fellow at the University of Manchester, UK. This work was also supported by the ERC Consolidator Grant *CMBSPEC* (No. 725456) as part of the European Union’s Horizon 2020 research and innovation program.

REFERENCES

- Alam S. et al., 2015, *The Astrophysical Journal Supplement Series*, 219, 12
- Alvey J., Sabti N., Escudero M., Fairbairn M., 2019, arXiv e-prints, arXiv:1910.10730
- Avelino P. P. et al., 2001, *Phys.Rev.D*, 64, 103505
- Battye R. A., Crittenden R., Weller J., 2001, *Phys.Rev.D*, 63, 043505
- Battye R. A., Moss A., 2014, *Physical Review Letters*, 112, 051303
- Bekenstein J. D., 1982, *Phys. Rev. D*, 25, 1527
- Bennett C. L. et al., 2013, *ApJS*, 208, 20
- Bernal J. L., Verde L., Riess A. G., 2016, *JCAP*, 1610, 019
- Bonifacio P. et al., 2014, *Astronomische Nachrichten*, 335, 83
- Chluba J., 2010, *MNRAS*, 402, 1195
- Chluba J., Thomas R. M., 2011, *MNRAS*, 412, 748
- Di Valentino E., Melchiorri A., Silk J., 2019, *Nature Astronomy*
- et. al. P., 2016, *A&A*, 594, A11
- Farhang M., Bond J. R., Chluba J., Switzer E. R., 2013, *ApJ*, 764, 137
- Galli S., Iocco F., Bertone G., Melchiorri A., 2009a, *Phys.Rev.D*, 80, 023505
- Galli S., Melchiorri A., Smoot G. F., Zahn O., 2009b, *Phys.Rev.D*, 80, 023508
- Gratton S., Lewis A., Efstathiou G., 2008, *Phys.Rev.D*, 77, 083507
- Hart L., Chluba J., 2018, *MNRAS*, 474, 1850
- Hütsi G., Hektor A., Raidal M., 2009, *A&A*, 505, 999
- Kaplinghat M., Scherrer R. J., Turner M. S., 1999, *Phys.Rev.D*, 60, 023516
- Knox L., Millea M., 2019, arXiv:1908.03663
- Kotuš S. M., Murphy M. T., Carswell R. F., 2017, *Monthly Notices of the Royal Astronomical Society*, 464, 3679
- Levshakov S. A., Ng K. W., Henkel C., Mookerjee B., Agafonova I. I., Liu S. Y., Wang W. H., 2019, *MNRAS*, 487, 5175
- Liu M., Huang Z., Luo X., Miao H., Singh N. K., Huang L., 2019, arXiv e-prints, arXiv:1912.00190
- Martins C. J. A. P., Vielzeuf P. E., Martinelli M., Calabrese E., Pandolfi S., 2015, *Phys. Lett.*, B743, 377
- Menegoni E., Archidiacono M., Calabrese E., Galli S., Martins C. J. A. P., Melchiorri A., 2012, *Phys.Rev.D*, 85, 107301

- Mota D. F., Barrow J. D., 2004, *Monthly Notices of the Royal Astronomical Society*, 349, 291
- Murphy M. T., Cooksey K. L., 2017, *Mon. Not. Roy. Astron. Soc.*, 471, 4930
- Negrelli C., Kraiselburd L., Landau S., Garca-Berro E., 2018, *International Journal of Modern Physics D*, 27, 1850099
- Planck Collaboration et al., 2014, *A&A*, 571, A16
- Planck Collaboration et al., 2016, *A&A*, 594, A19
- Planck Collaboration et al., 2015a, *ArXiv:1502.01589*
- Planck Collaboration et al., 2015b, *A&A*, 580, A22
- Planck Collaboration et al., 2018a, *ArXiv:1807.06209*
- Planck Collaboration et al., 2019a, *arXiv e-prints*, *arXiv:1907.12875*
- Planck Collaboration et al., 2018b, *arXiv e-prints*, *arXiv:1807.06210*
- Planck Collaboration et al., 2018c, *arXiv e-prints*, *arXiv:1807.06205*
- Planck Collaboration et al., 2019b, *arXiv e-prints*, *arXiv:1906.02552*
- Poulin V., Smith T. L., Karwal T., Kamionkowski M., 2019, *Phys.Rev.Lett.*, 122, 221301
- Riess A. G., Casertano S., Yuan W., Macri L. M., Scolnic D., 2019, *Astrophys. J.*, 876, 85
- Riess A. G. et al., 2011, *The Astrophysical Journal*, 730, 119
- Riess A. G., et al., 2016, *Astrophys. J.*, 826, 56
- Rubiño-Martín J. A., Chluba J., Fendt W. A., Wandelt B. D., 2010, *MNRAS*, 403, 439
- Scóccola C. G., Landau S. J., Vucetich H., 2009, *Memorie della Societ Astronomica Italiana*, 80, 814
- Shaw J. R., Lewis A., 2010, *Phys.Rev.D*, 81, 043517
- Smith T. L., Grin D., Robinson D., Qi D., 2019, *Phys. Rev. D*, 99, 043531
- Uzan J.-P., 2003, *Reviews of Modern Physics*, 75, 403
- Uzan J.-P., 2011, *Living Reviews in Relativity*, 14, 2

APPENDIX A: EXTRA MARGINALISED RESULTS

For transparency, in Fig. A1, we show the full parameter constraints for Λ CDM parameters and m_e when BAO and R19 data is added.

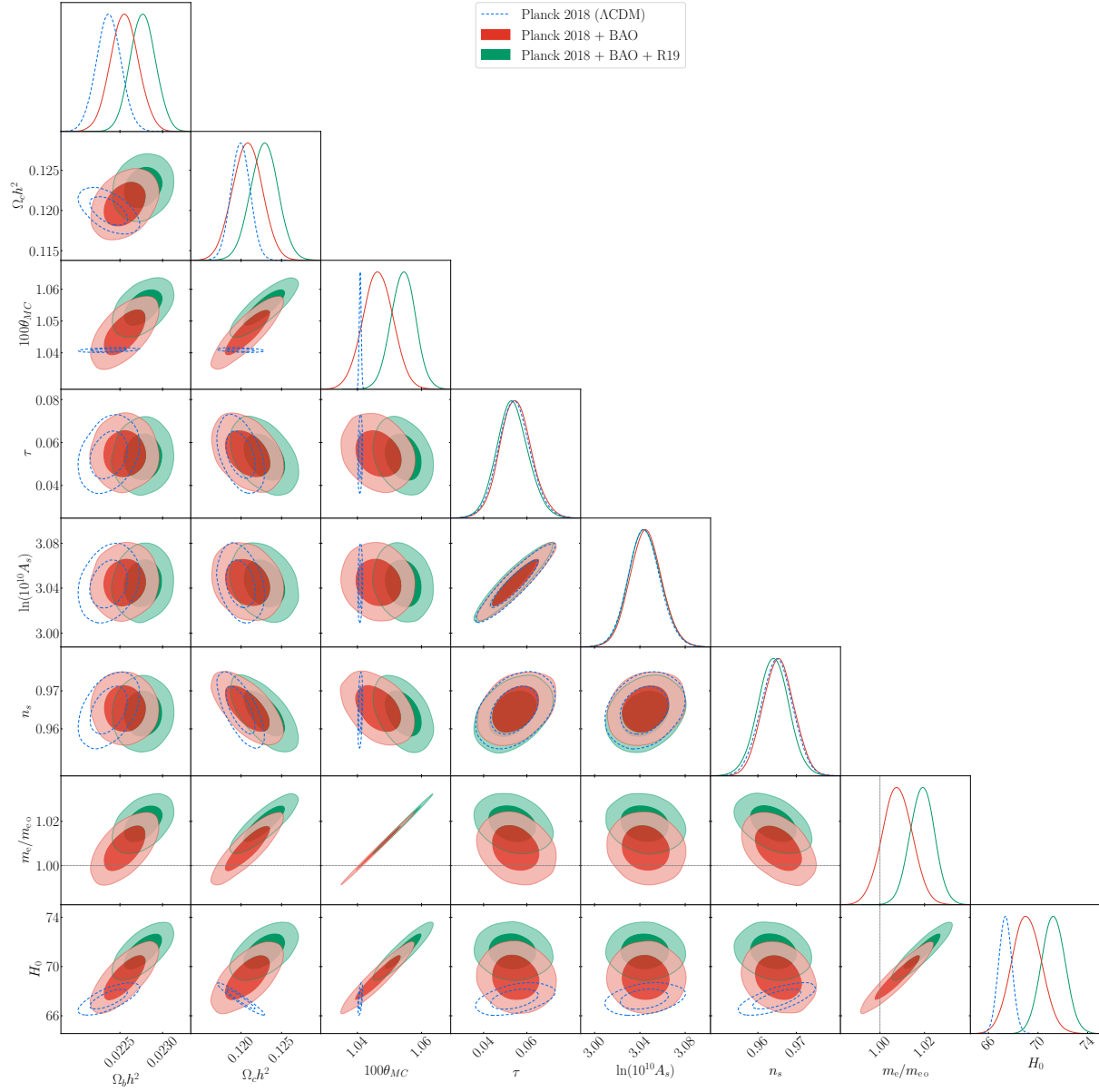


Figure A1. Fully marginalised results from *Planck* + BAO and *Planck* + BAO + R19 and variations of m_e with CMB only as a reference (blue-dashed). This figure includes contributions from $\{\tau, n_s, \ln(10^{10} A_s)\}$ which are effectively decoupled from m_e . The Λ CDM value of $m_e = 1$ is added as a dashed line.